Interpretation of stall precursor signatures-stable instabilities

Christoph Brandstetter[1*], *Xavier* Ottavy[1†], and *Sina* Stapelfeldt[2‡]

[1]Université de Lyon, Ecole Centrale de Lyon, CNRS, LMFA, UMR 5509, F-69134, ECULLY, France
[2]Imperial College, Department of Mechanical Engineering, London, United Kingdom

Abstract. A specific phenomenon that has been observed in many experimental studies on turbomachinery compressors and fans is discussed under the term "rotating instabilities". It is associated to a local aerodynamic phenomenon, typically occurring in the tip region at highly loaded near stall conditions and often linked to blade vibrations. Even though the effect has been discussed over more than two decades, a very ambiguous interpretation still prevails. A particular problem is that certain signatures in measurement data are often considered to characterize the phenomenon despite possible misinterpretations. The present paper illustrates that a specific image of a pulsating disturbance that has been established in the 1990s needs to be reconsidered. At the example of a recent investigation on a composite fan the difficulties concerning sensor placement and post-processing techniques is discussed with a focus on spectral averaging, isolation of non-synchronous phenomena and multi-sensor cross-correlation methods.

Nomenclature

A	Amplitude
bpf	Blade passing frequency
EO	Engine Order
N_α	Circumferential mode order of aerodynamic disturbance
N_v	Circumferential Mode Order of blade vibration pattern (Nodal Diameter)
NSV	Non Synchronous Vibration
p	Pressure
SWFT	Sliding Window Fourier Transformation
ω	Angular frequency
Ω	Angular velocity
θ	Circumferential Coordinate

Subscripts

a	Aerodynamic or acoustic disturbance
b	Rotor blades
m	Modulation
r	Rotor
v	Vibrator
05	half-life

Superscripts

s	stationary frame of reference
r	rotating frame of reference

1 Introduction

The onset of rotating stall in turbomachinery compressors has been extensively studied and has various forms of precursors. Typical for modern high-speed axial compressors and fans is the occurrence of short-length scale aerodynamic disturbances appearing close to the casing and propagating around the circumference before the establishment of a classical rotating stall cell. This type of disturbance is often referred to as a "spike", a small vortex with radial rotation axis. These vortices travel around the circumference at a fraction of the rotor speed that is close to the angular velocity of a rotating stall cell.
Certain types of compressors develop similar aerodynamic disturbances in the tip region, which propagate around the circumference at stable operating conditions far from the onset of rotating stall. The disturbances are often inhomogeneous around the circumference and comprise a multitude of wavelengths.
In many experimental studies it was found that the propagation speed of these disturbances is largely independent of the local wavelength and close to that of rotating stall precursors or cells.

* *Christoph* Brandstetter: christoph.brandstetter@ec-lyon.fr
† *Xavier* Ottavy: xavier.ottavy@ec-lyon.fr
‡ *Sina* Stapeldeldt: s.stapelfeldt@imperial.ac.uk

When measured in the stationary frame of reference, these phenomena manifests themselves as a range of frequency peaks in the pressure spectrum. The peaks are located at a fraction of the blade passing frequency and often referred to as a "broadband hump".
A typical spectrum, showing this type of disturbance has been published by Baumgartner et al. in 1995 [1] and is shown in Fig. 1. In this and other publications from the era, the term "Rotating Instabilities" has been established. The spectrum shows not only a broadband disturbance (hump) around 30% of the BPF but also individual peaks with a narrow spacing. In addition, this signature is modulated with the blade passing frequency and its harmonics, showing left and right-handed sidebands. The source of the disturbance has been described as a form of vortex-shedding.

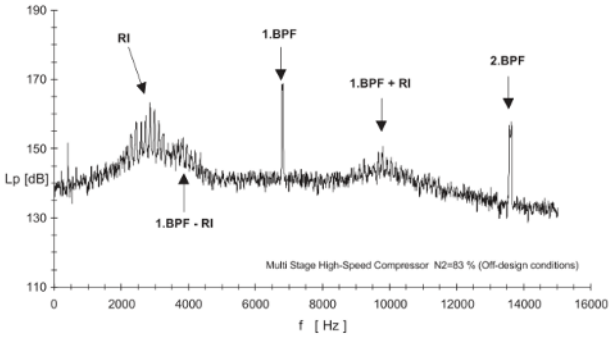

Fig. 1. Pressure spectrum from Baumgartner et al. [1]

In [1] a link to non-synchronous blade vibrations in structural eigenmodes has been drawn. Based on the assumption that the spacing of the peaks in the spectrum corresponds to subsequent integer wave numbers, the frequency spacing between two peaks corresponds to the angular velocity of the disturbance. Since not all frequencies in the stationary and rotating frame could be explained in terms of purely travelling waves, the authors concluded that the disturbances must also be pulsating in their own frame of reference. . The image of a rotating loudspeaker was used to explain the coherence of the pressure disturbances with the structural vibration modes. This image was supported by the work of Kameier and Neise [2] who implemented a rotating loudspeaker into a fan-test rig and confirmed the theoretical assumptions concerning measured frequencies and compared them to experimental data from a fan. It was observed, that within the relevant frequency range of the spectrum, a linear phase evolution is present in inter-spectra of circumferentially distributed sensors.
Numerous studies on the phenomenon have been conducted afterwards, where the characteristic of "frequencies in the source frame of reference" was used as an identifying feature for the phenomenon. This partly lead to intense discussions on the semantics ("Rotating Instability" vs. "Part Span Stall" etc.) and the underlying aerodynamic effect (leading edge vortex separations , fluctuations of the tip leakage vortex) [3,4].
In the present paper we will show, that the image of a pulsating source mechanism is not necessary to explain the measured spectra but rather misleading.
Instead, experiments indicate that widely stable or decaying disturbance patterns are convected at constant speed around the circumference.
Furthermore, the quantitative interpretation of frequency peaks in measured spectra is extremely difficult. Physical interactions between structural vibrations, propagating acoustic modes and the convected aerodynamic disturbances can cause frequency lock-in and lead to erroneous interpretations. It is shown how post-processing parameters and measurement methods have significant impact on the interpretation.
A method based on multi-sensor correlation for the characterization of specific modes is proposed.

2 Fundamentals

Propagating disturbances in turbomachines can be subdivided into convected disturbances and acoustic waves. In all cases, the disturbance at a specific axial position and constant radius can be described as a superposition of harmonic waves.

Experimental observations have shown that the propagation of stall precursors such as small vortices in the tip region occurs at a widely constant speed Ω_a^S independent of their spatial extension. This is consistent with vorticity disturbances travelling with the mean flow.

For the simple case of a freely **convected disturbance** with inhomogeneous or periodic spatial pattern the associated pressure field in the stationary frame of reference can be described as:

$$p^S(\theta,t) = \sum_{N_a=-\infty}^{\infty} A_{N_a}\, e^{i(N_a\theta - N_a\Omega_a^S t)} \quad (1)$$

For two consecutive wave numbers N_a the angular frequency in the stationary frame of reference is given as:

$$\omega_1^S = \mathrm{N_{a,1}}\Omega_a^S\,;\ \omega_2^S = \left(\mathrm{N_{a,1}}+1\right)\Omega_a^S (2)$$

Hence the propagation speed can be determined as:

$$\Omega_a^S = \omega_2^S - \omega_1^S \quad (3)$$

A series of equally distributed peaks for arbitrary asymmetric or periodic, but temporarily stable or slowly decaying disturbances, therefore produces a spectrum with distinct peaks, spaced by Ω_a^S. The phase change measured with two sensors between positions θ_1 and θ_2 will be linear according to: $\varphi_{12} = N_a(\theta_2 - \theta_1)$.

Adding a layer of complexity, this pattern can be modulated through interaction with external feedback mechanisms like acoustic duct modes. Modulation with planar modes can be written as:

$$\mathrm{p^S(\theta,t)} = \sum_{\mathrm{N_a}=-\infty}^{\infty} \mathrm{A_{N_a}}\, \mathrm{e^{-i\omega_m^S t} e^{i(N_a\theta - N_a\Omega_a^S t)}} \quad (4)$$

with ω_m^S representing the frequency of the modulation mechanism, for example that of a planar acoustic duct resonance. This representation is similar to that in [1], eq. (11) and [2] where ω_m^S is described as a characteristic frequency of the rotating instability.
The specific case of scattering with N_b rotor blades and its h harmonics is represented as:

$$p_m^S(\theta,t) = \sum_{N_a=-\infty}^{\infty} A_{n,N_a}\, e^{\pm i h N_b \Omega_r^S t} e^{i(N_a\theta - N_a \Omega_a^S t)} \quad (5)$$

which leads to sidebands of the blade passing frequency $bpf \pm N_a\Omega_a^S$ (where $bpf = N_b\Omega_r^S$).

In contrast, **disturbances generated by a vibration pattern** in the rotating frame produce a different signature. Blades vibrating in a specific eigenmode with frequency ω_v^R in the rotor frame and a circumferential vibration pattern with nodal diameter N_v will produce aerodynamic disturbances in the stationary frame of reference with the frequency:

$$\omega_{N_v}^S = \omega_v^R + N_v\Omega_r^S \quad (6)$$

As typically not only a single circumferential mode order is present, the frequency signature in the stationary frame of two consecutive nodal diameters will produce peaks with a spacing of the shaft frequency Ω_r^S, or one Engine Order.

For swirling **acoustic duct modes**, the phase velocity Ω_a^S cannot be considered constant and independent from the mode order.. Assuming a narrow duct, the propagation characteristics of homogeneous acoustic modes can be derived by calculating the eigenvalues of the wave equation as lined out by Tyler and Sofrin [5] or Camp [6]. It is found that a mode is propagative with negligible amplitude decay in axial direction (cut-on) if the phase velocity relative to the flow exceeds the local speed of sound; otherwise it is evanescent with exponentially decaying amplitude. This means that due to rising swirl in a rotor, it is possible for co-rotating modes to only be propagative in the upstream direction and vice versa. This effect is of great interest for acoustic resonance and acoustically driven flutter based on trapped modes [7,8]. In context of this paper it is important, that modes above a critical frequency (cut-on frequency) will not decay exponentially in axial direction and propagate with an angular phase velocity that exceeds the speed of sound relative to the flow. Co-rotating modes hence propagate faster than the angular rotor velocity for subsonic or transonic machines. Critical modes for acoustic resonance and flutter are those, which are cut-on only in one axial direction of the rotor [9].

For both cases, convected disturbances and acoustic modes an effect described as “lock-in” may occur if two physical phenomena interact [10], for example, it has been shown, that the frequency of free vortex shedding can be altered through significant vibration of the disturbance generating body, if the oscillation frequency is close to the free shedding frequency (Strouhal frequency). This frequency lock-in becomes more effective at high oscillation amplitudes. The same has been shown for acoustic forcing in [11].

In turbomachinery compressors, the effect denoted as Non-Synchronous-Vibration [12] relies on a comparable effect: Initially randomly distributed disturbances, which are being convected circumferentially at highly loaded operating conditions, can be modified through blade vibration, when the vibration pattern causes a lock-in of the phase of vortex separations from the blades [13]. In a narrow range, the group propagation velocity of the aerodynamic disturbance can then adapt to the phase velocity of the structural vibration pattern and form a coherent interaction pattern with distinct wave numbers. As a result, the measured frequency of the disturbance for a specific wave number shifts with the lock-in of the propagation speed [14]. This is illustrated in Fig. 2, showing the shift of the propagation speed of convected disturbances during a transient throttling maneuver into NSV [13].

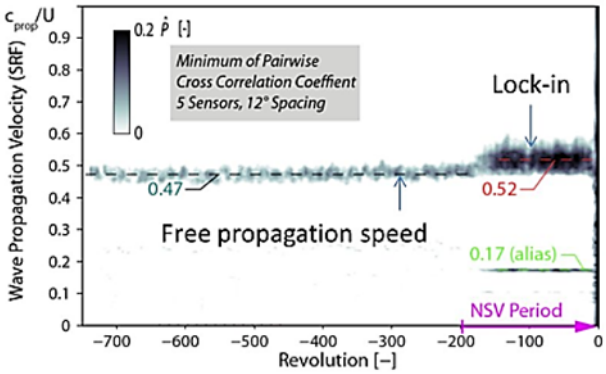

Fig. 2. Lock-in of group propagation speed after onset of nsv; from [13]

The same applies to resonance between an unstable aerodynamic phenomenon (like vortex shedding) with a propagating acoustic duct mode [6, 7, 11] , since the frequency of a resonating mode is fixed for specific wave numbers by the acoustic propagation conditions and the duct geometry. Trapped acoustic duct modes can reach amplitudes of the order of 15-20 kPa in axial compressors and can hence be a very effective feedback mechanism for aerodynamic phenomena and structural vibrations [15, 16].

3 Analysis of transient measurement

The most common method to analyze transient or periodic phenomena in turbomachines is to perform a Fourier transformation. As non-synchronous effects are typically not strictly periodic, the selection of processing parameters is of great importance. A typical approach for transient investigations is to perform a sliding window Fourier transformation (SWFT). Without going into spectral density estimations and well understood problems concerning signal acquisition (resolution, transfer function, aliasing, noise, etc.) and methods to reduce transformation artefacts like spectral leakage (application of window functions) the influence of three particular parameters will be discussed in the following as they have an immense effect on the interpretation:

a) Subtraction of ensemble average
b) Window length / spectral averaging
c) Sensor position

The first method that has proven effective to isolate non-synchronous phenomena is the subtraction of a sliding average from the temporal signal before performing a spectral analysis. By using a simultaneously recorded signal of the shaft position

(trigger), an ensemble average of several revolutions is calculated and afterwards subtracted from each revolution [17].
If the shaft speed varies during the measurement, interpolation may be necessary. As a result, all phenomena that occur periodically with the rotor revolution are removed, including steady non-axisymmetric disturbances and rotor-stator interactions, which all occur at integer engine orders.

The method varies fundamentally from a bandstop filter at integer engine orders, since it only removes signals that appear in subsequent revolutions but not those of a specific frequency that only last for a short duration. This point is important, because non-synchronous peaks within a spectrum may be close to integer engine orders, which can lead to merging of two completely different effects in the spectrum of an individual sensor.

This is illustrated at the example of a measurement at a part-speedline of a modern composite material fan at a stable operating point near stall [18] .

Fig. 3 a) shows averaged spectra of a continuous measurement during 10s of a sensor near the leading edge for a SWFT window length of 25 revolutions (frequency resolution 0.02 EO) with and without subtraction of a sliding ensemble average of 25 revolutions. A Hamming function was applied to each individual window. Clearly, synchronous peaks are effectively eliminated (EO 2-5,8,11) and particularly the blade passing frequency at EO16. The non-synchronous content of the signal remains unaffected.

The chosen window length is of equal importance. Fig. 3 b) represents the same measurement but with a window length of 250 revolutions.

Focusing on the broadband disturbance, amplitude and peak distinction are more prominent for the shorter window with reduced frequency revolution. As can be seen in the plots, the amplitude of the synchronous signal with respect to the non-synchronous disturbance is much higher for the longer window length. This means that solely through a longer transformation window, the non-synchronous activity can be underestimated.

To demonstrate the effect of axial sensor position, Fig. 4 presents the spectra for different window sizes between 5 and 250 revolutions before averaging for four locations. Position c) corresponds to the graph shown in Fig. 3 a). The disturbance is obviously highest near the leading edge of the fan. With rising window length, the average amplitude is reduced, indicating that the individual disturbances are not strictly periodic but decay temporarily.

However this does not apply equally to all peaks within the disturbance, for example the peak at EO8.46 is less affected upstream (position a) and has almost constant amplitude for a window length of 5 and 25 revolutions, indicating a stronger periodicity or more stable disturbances. Near the trailing edge (position d) this peak is much less dominant compared to upstream positions.

At position c) the peak at EO8.04 is only visible for the higher window length, whereas it becomes the most dominant peak at position b).

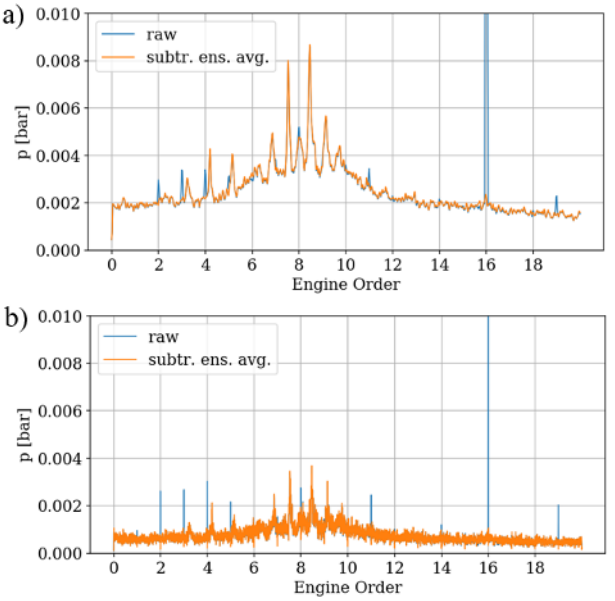

Fig. 3. Frequency spectra of fan operating near stall with and without subtraction of ensemble average; a) SWFT window 25 rev, b) SWFT window 250rev

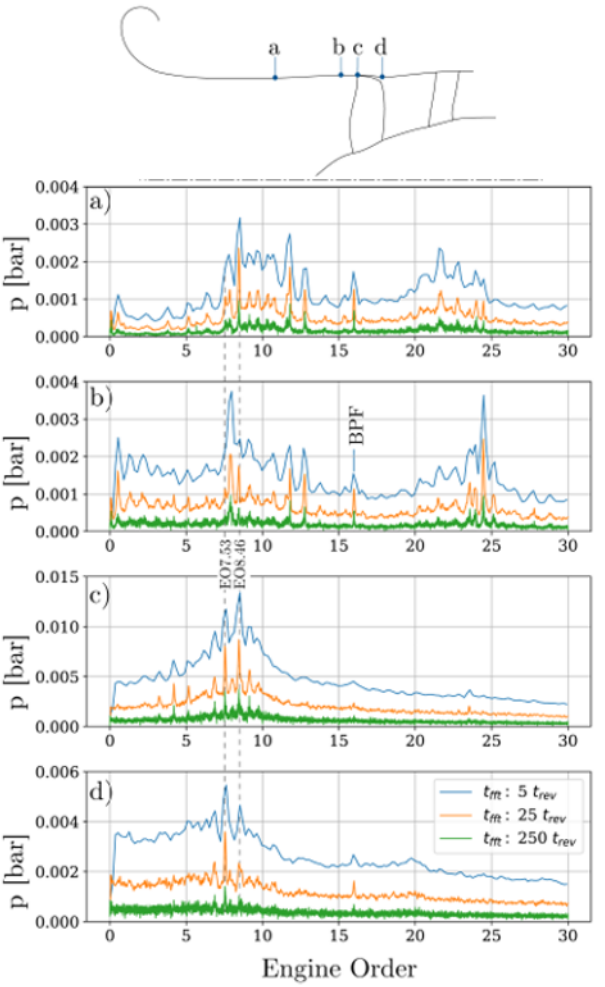

Fig. 4. Pressure spectra of fan operating near stall at different axial sensor positions and varying SWFT window; subtracted ensemble average

At the trailing edge, the signature is still present but its amplitude is reduced to approximately 40%.

Approximately one axial chord upstream, the amplitude has reduced significantly compared to low-frequency fluctuations. Far upstream, the shape of the disturbance has altered; merely frequencies above engine order 7 are dominant.

These results indicate that a quantitative interpretation based on these spectra is difficult as 3 parameters have such significant influence, not only on the amplitude but also on the general presence of spectral peaks.

To analyze further the composition of the disturbance without relying on Fourier transformation, the presence of circumferentially distributed sensors can be exploited. With the results indicating that the disturbances are not periodic and weakly coupled around the circumference, harmonic analysis is obviously not targeted. Besides classical cross-spectral methods, it is possible to combine windowed cross correlations of different sensor pairs. The method has been described in [13].

By transforming the cross correlation vector based on the acquisition sampling rate into a propagation speed of a rotating disturbance [17], a minimum correlation for each window and sensor pair can be derived to remove aliased peaks. Inhomogeneous sensor spacing is beneficial. This method does not require sinusoidal disturbances but only a disturbance pattern that remains stable as it traverses the circumferentially distributed sensors. The window length itself has no significant influence on the result.

Applying this method to the given measurement - without applying a spectral filter but with removed ensemble average - the results presented in Fig. 5a) are derived. At the position close to the leading edge, a dominant group propagation speed of Ω_a^S=0.53Ω_r^S is observed, including all disturbances of different wavelengths.

To analyze the characteristics of each individual peak in the measured spectra, a band-pass filter in a range of ± 0.2 EO around each peak was applied before performing the cross correlation. Exemplarily, for the peaks at EO 7.53 and EO11.79 the derived minimum correlation value of circumferentially distributed sensors at position b) is presented in Fig. 5 b) and c).

It can be seen, that for the peak at EO7.53 a dominant propagation speed of Ω_a^S=0.58Ω_r^S is derived. Based on this value, the circumferential wave number is N_a=7.53/0.58=13. This speed is typical for a convective transport mechanism as described in [14] and [18]. For the peak at EO 11.79 however, a propagation speed of Ω_a^S=1.48Ω_r^S is determined, indicating a co-rotating acoustic wave with a circumferential mode order of N_a=11.79/1.48=8.

In order to derive structural vibration patterns which may be in interaction with the aerodynamic or acoustic disturbances, the same method can be applied to rotor-strain gauges on different rotor blades. Filtered on specific vibration eigenmodes, the dominant nodal diameter can be calculated. Fig. 6 presents the transient results for the given measurement, filtered on the 3rd blade vibration mode at EO_{rel}=5.46, while entering rotating stall at revolution 0, indicating that a dominant nodal diameter of N_v=3 is present in the pre-stall phase. More detail on this interaction is given in [18].

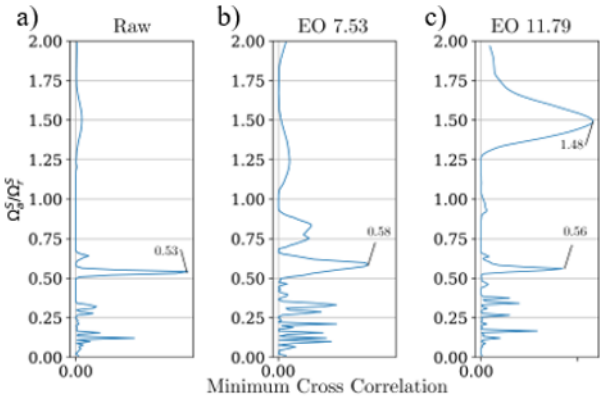

Fig. 5. Minimum of multi-sensor cross correlation for measurement near stall; a) unfiltered data; b) and c) band-pass filtered on specific modes

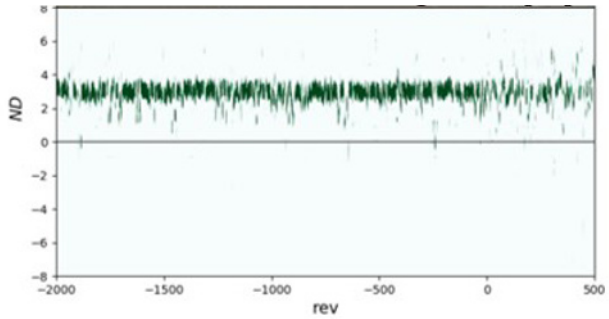

Fig. 6. Minimum cross correlation value of multiple rotor strain gauges before and during stall inception; filtered on vibration mode 3

Using the described method, a detailed analysis of the measured spectra for the composite fan operating near stall is possible. Fig. 7 shows the spectrum for all wall pressure sensors (axial positions marked as black triangles at the bottom of the figure). The SWFT window size is 25 revolutions and a sliding ensemble average of each 25 revolutions has been subtracted.

Clearly the strongest non synchronous activity is observed around the rotor leading edge, comprising broadband noise and individual peaks as already discussed. This illustration emphasizes, how the majority of the disturbances decays axially, except for some individual peaks which remain at constant amplitude in the upstream direction (i.e. EO8.46, 11.79, 12.76 and 24.46). For a series of dominant peaks, Table 1 presents the results of the waveform analysis based on multi-sensor correlation. For most peaks below EO10, a dominant propagation speed around Ω_a^S=0.55Ω_r^S is determined (column 3). By using:

$$N_a = \omega^S / \Omega_a^S \quad (7)$$

The circumferential mode order N_a presented in the second column is derived. It can be seen that some peaks can be assigned to consecutive wave numbers with almost constant propagation speed close to the average group propagation speed (N_a11/12/13 and N_a17/18).
The highest amplitude at the leading edge position is measured for the peak at EO8.46 with a dominant

propagation speed of Ω_a^S=2.82Ω_r^S, corresponding exactly to the vibration pattern of the dominant forward traveling Nodal Diameter 3 based on the 3rd blade eigenmode, which has a frequency of $EO_{M3}^R = \frac{\omega_{M3}^R}{\Omega_R^S} = 5.46$, measured with the strain gauges (compare Fig. 6). It is hence evident, that the measured peak at EO7.53 corresponding to an aerodynamic disturbance with wave number N_a13 is in resonance with the aliased structural vibration pattern of the fan with $N_b = 16$ blades :

$$N_b - N_a = N_v \rightarrow 16 - 13 = 3 \quad (8)$$

with the frequency:

$$EO16\text{-}EO7.53 = EO8.46 \quad (9)$$

This synchronization of an aerodynamic disturbance with a structural vibration pattern is described in literature as "Non-Synchronous-Vibration" [14]. The acoustic signature of the vibration pattern (EO8.46/N_v3) is propagative (cut-on) in both axial directions of the duct, explaining the non-decaying amplitude visible in Fig. 4.

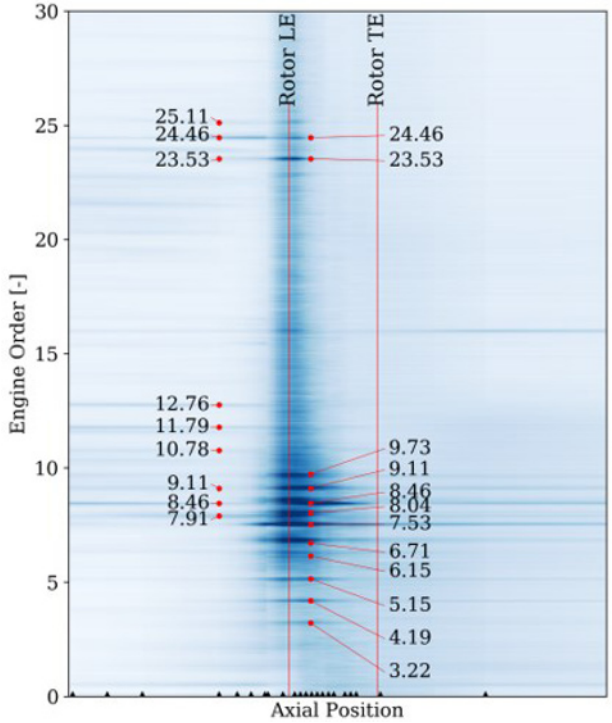

Fig. 7. Wall pressure spectrum of fan operating near stall, subtraction of ensemble average; SWFT window 25rev

Further correspondence between structural modes and aerodynamic disturbances is found for the peaks EO3.22, EO4.19 and EO5.15, which can be associated to vibration patterns of the second blade eigenmodes $EO_{M2}^R = 3.8$ in Nodal diameters N_v9(-7), 7 and 8 as denoted in column 4 of Table 1.

The peaks at EO10.78, EO11.79 and 12.76 hence represent acoustic signatures of these patterns according to eq. 6. In contrast to the signature of peak EO8.46, those modes are cut-on only in the upstream direction with Ω_a^S/Ω_r^S≈1.5.

The peaks above the blade passing frequency correspond to scattered modes with the first and second blade passing harmonic according to eq. 5, as denoted in Table 1.

Table 1. Decomposition of spectral peaks

EO^s	N_a	Ω_a^S/Ω_r^S	Description	cut-on upstr.	t_{05}
3.22	7	0.460	NSV M2 N_v -7	0	0.5
4.19	8	0.524	NSV M2 N_v 8	0	0.8
5.15	9	0.572	NSV M2 N_v 7	0	0.7
6.15	11	0.559	free conv.	0	0.4
6.71	12	0.559	free conv./NSV	0	0.4
7.53	13	0.579	NSV M3 N_v 3	0	1.8
8.04	15	0.536	free conv.	0	0.8
8.46	3	2.820	Acoust. M3 N_v 3	1	2.7
9.11	17	0.536	free conv.	0	0.4
9.73	18	0.541	free conv.	0	0.6
10.78	7	1.540	Acoust. M2 N_v7	1	1.3
11.79	8	1.474	Acoust. M2 N_v 8	1	1.1
12.76	9	1.418	Acoust. M2 N_v 9	1	2.6
23.53	29	0.811	N_b16+N_a13	0	0.7
24.43	19	1.286	2xN_b16-N_a13	1	2.6
25.11	33	0.761	N_b16+N_a17	0	0.6

Considering the cross-spectral coherence an estimation of the decay rate of individual disturbances can be derived as described in the appendix. The last column in Table 1 shows the derived half-life for the individual modes, showing an average value of 0.4-0.8 revolutions for the convected disturbances which are not locked in. Acoustic modes and structural interaction modes are more coherent and stable, as already indicated in Fig. 4 regarding the influence of the SWFT window. However, an average half-life of the convected disturbances of approximately 0.5 revolutions cannot be considered unstable, particularly as the machine is operated at highly loaded conditions.

In Fig. 8 a) the measured propagation speed (via cross correlation of the band-pass filtered raw data), is plotted against the corresponding wave number N_a. Additionally, the phase velocity of the blade vibration modes 2 and 3 (or that of the aliased mode $N_a = N_b - N_v$) is presented. It can be seen, that for wave number 13, an exact correspondence is present with the structural mode $\left(\frac{\Omega_a^S}{\Omega_r^S} = 0.579\right)$, whereas for higher order modes, the propagation speed is slightly lower $\left(\frac{\Omega_a^S}{\Omega_r^S} = 0.53 - 0.54\right)$. Same applies for the two peaks at wave number N_a11 and 12, which don't match exactly with the structural mode. The aerodynamic disturbances of wave number 7 to 9 instead exactly correspond with vibration mode 2. This correspondence can also be seen in Fig. 8 b) showing the measured engine order against the wave number with a peak spacing of one engine order for wave numbers 7 to 9 (see eq.6).

Comparing these results to the amplitude of the vibration modes, presented in Fig. 8 c), the aeroelastic phenomenon can be clearly interpreted as follows: Multiple disturbances of different wave-lengths propagate around the circumference with an

aerodynamically determined group velocity of 0.53-0.54 and excite several vibration modes. A lock-in phenomenon occurs for a wave number of 13, leading to a shift of the propagation speed to adapt with the vibration pattern of vibration mode 3 in Nodal Diameter 3. Same applies to the weaker interaction with vibration mode 2. Disturbances of shorter wavelength (N_a15 to 19) convect freely.

This analysis shows, that only for a few peaks in the spectrum, the peak spacing corresponds to the actual propagation speed of the aerodynamic disturbances. Several peaks represent acoustic signatures of vibration modes or modulations. A dominant peak (EO7.53) generally corresponds to a convected disturbance but has locked in to a vibration mode and hence shifted in frequency. Specific wave numbers (10 and 14) are not visible in the measurements due to lock-in with the nearest NSV-interaction mode.

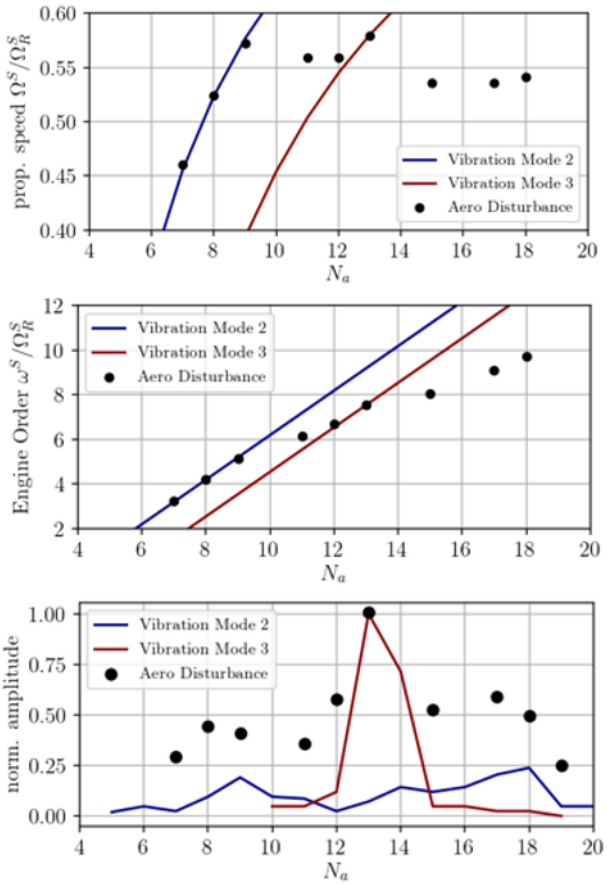

Fig. 8. Characteristics of dominant modes in dependency of aerodynamic wave number

Summarizing, the occurrence of peaks in a measured pressure spectrum may result from manifold interaction effects. In order to determine the characteristics of a specific mode it is not at all sufficient to argue based on peak spacing, as subsequent peaks are caused by different effects and can be shifted due to lock-in mechanisms. However, the fact that several peaks rely on constant convective propagation of aerodynamic disturbances can be used to model the phenomenon.

4 Modeling

For a case of a high speed compressor that suffers from NSV in a comparable way as the fan presented in this study a semi-analytical model for the prediction of the fluid-structure interaction has been developed and described in [14]. The time marching model comprises a one-dimensional term for the convection of free circulation around the circumference which is generated by twisting blade motion and inversely leads to modal forcing on the blades, which are modeled as oscillating masses as schematically shown in Fig. 9. Calibrated with transient CFD-simulations the model is able to predict critical NSV-modes, including the described lock-in phenomenon. The conservation term for the aerodynamic disturbance in the model can also be used to integrate random distortions propagating with a constant speed as described in this paper.

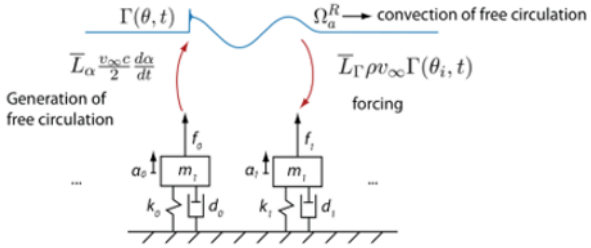

Fig. 9. Schematic of semi analytical model; blades represented as mass oscillators; aerodynamic disturbance generated by blade oscillation convected from blade to blade causing modal forcing; from [14]

Applied to the presented case, with the lumped mass-oscillators tuned to vibration mode 3 and the disturbance propagation speed set to 0.54, the model derives the results presented in Fig. 10.

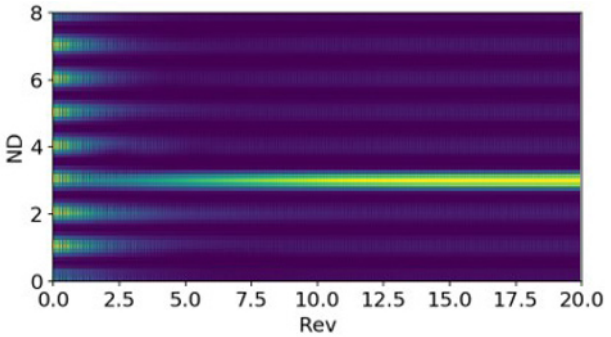

Fig. 10. Temporal development of structural nodal diameter in semi-analytic model

After several revolutions, the rotor develops a Nodal Diameter 3 pattern with a dominant aerodynamic wave number of 13 and a locked-in propagation speed of 0.57. If a random disturbance pattern is imposed as initial condition, the frequency spectrum after several revolutions contains multiple peaks corresponding to different wave numbers, compared to the experimental results in Fig. 11. It can be seen, that all peaks, corresponding to free propagating disturbances and those locked in to vibration mode 3 are well presented in the model. As vibration mode 2 is not modeled, the peaks at

low engine orders are therefore not locked in. The model can hence be used to facilitate the interpretation of measurement results and estimate lock-in effects.

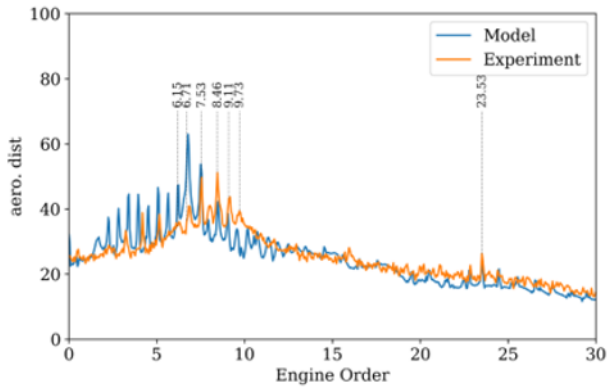

Fig. 11. Comparison of measurement and semi-analytic model spectra, model tuned on vibration mode 3, propagation speed Ω_a^S=0.54Ω_r^S, amplitudes normalized

This is demonstrated at the example of one of the first publications on Non-Synchronous-Vibrations and "Rotating Instabilities" by Baumgartner et al. [1]. In this publication, measured pressure spectra are presented, as depicted in Fig. 12, showing multiple peaks with a dominant peak at engine order 13.46. The authors used two adjacent peaks to determine the propagation speed of the dominant mode to 0.62 Ω_r^S. Considering the blade vibration frequencies of two modes, the authors also determined possible interaction modes, and suspected a characteristic frequency of the "rotating instabilities" as the responsible phenomenon for the excitation of the vibration modes.

Using exactly the same calibration values for circulation generation and modal forcing as for the presented fan, the semi-analytical model was applied to the case presented by Baumgartner et al, merely the blade number (27), vibration eigenfrequency (EO13.44) and propagation speed were adapted to the values given in the paper.

With pre-imposed random disturbance, the model develops the spectrum presented in Fig. 12 b) in comparison to the measurement results from [1]. Clearly, all peaks observed in the measurements are well represented in the model results and can be associated to wave numbers of the aerodynamic disturbances. Coherent structural interaction (NSV) between aerodynamic disturbances of wave number Na13 with the blade vibration mode in a pattern of N_v6 causes the dominant peak. Random excitation of multiple nodal diameters leads to further peaks which are not in resonance but visible in both, the model results as in the measurements (i.e. N_v5 and N_v7).

As the model only contains a disturbance term, that is constantly propagated and interacts with the blades, without any consideration of modulation in the sense of eq. 4, it is clear that it is not necessary to consider a characteristic frequency of the disturbances (rotating instabilities) to explain the phenomenon. All spectral peaks, the excitation of the critical vibration pattern and hence the emphasized peak at the coherent mode are present in the model.

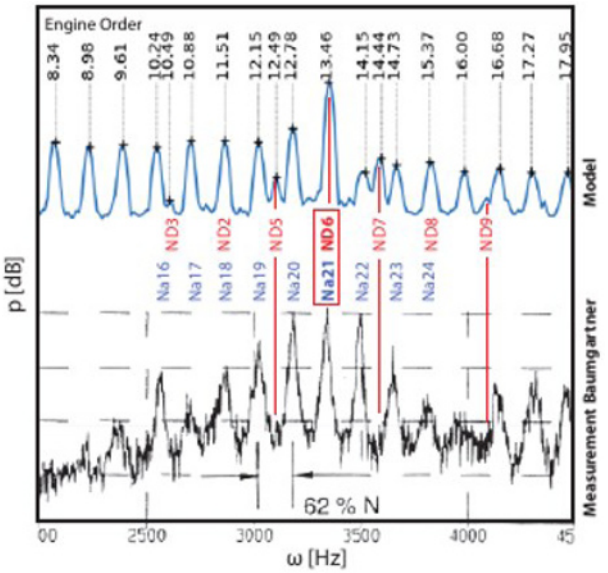

Fig. 12. Comparison of measured spectra from Baumgartner et al. [1] and semi-analytic model (Model SB)

Moreover, the most coherent spectrum compared to the measurement was found for a propagation speed in the model set to Ω_a^S=0.637Ω_r^S deviating slightly from the peak spacing of 0.62 derived from the peak spacing and denoted in Fig. 12.

The proposed procedure to analyze measurements towards non-synchronous phenomena near the stability limit can be summarized as follows with recommended parameters:

1. Subtraction of sliding ensemble average (5-50 revolutions)
2. Sliding Window Fourier Transformation (10-50 rev depending on required resolution, averaging of spectra)
3. Multi-sensor cross correlation to derive dominant propagation speed of raw signal and band-pass filtered signal of spectral peaks to determine circumferential mode orders (correlation window 3-10 revolutions, depending on dominant propagation speed and sensor spacing)
4. Determination of possible convective and acoustic phenomena, analysis of cut-on conditions based on averaged flow conditions upstream and downstream of relevant rotor or stator [6].
5. If available, comparison with blade vibration measurement to determine aeroelastic interaction modes.
   Otherwise estimation of structural eigenfrequencies and identification of possible interaction peaks.
6. Consideration of reduced order model to validate possible lock-in effects and determination of dominant group propagation speed.

5 Conclusion

The presented study has shown that a robust analysis of measurements near the stability limit is sensitive to the used methodology and requires a thorough procedure to account for multi-physical interaction mechanisms. Generation of pressure spectra is very sensitive to sensor integration (position and transfer function) and post-processing parameters (window length, subtraction of ensemble average, spectral averaging).

A procedure to achieve a detailed decomposition of non-synchronous modes was proposed. Implementation requires that unsteady pressure sensors are integrated at different axial positions as specific modes may be present only in a narrow range. One stage needs to be instrumented with at least 3 non-homogeneously spaced circumferential sensors to enable multi-sensor correlation, preferably close to the leading edge.

The interpretation of measurements based solely on peaks in measured spectra is generally misleading, because lock-in with structural vibration or acoustic modes is possible, and an overlap with forced response and Rotor-stator interactions as well as modulations with harmonics of the blade passing frequencies may be present. It was shown at the specific example of a modern low-transonic fan that a “typical” pre-stall pressure spectrum contains peaks associated to pure aerodynamic disturbances, locked-in peaks due to non-synchronous vibrations, acoustic signatures of vibration patterns and modulations with the rotor blades.

Lastly, it was shown, that the established interpretation of pre-stall disturbances as an aerodynamic phenomenon with a characteristic source frequency must be reconsidered. Measured spectra can be explained by a stable or slowly decaying aerodynamic disturbance pattern that is convected at constant speed around the circumference but not to be confused with rotating stall [14]. The analysis has shown that for the studied case the non-locked-in disturbances decay with an average half-life of between 0.4 and .8 revolution and should hence not be considered a rotating instability.

6 Acknowledgments

The presented research was supported through the European Unions Seventh Framework Programme for research, technological development and demonstration, ENOVAL, grant agreement no 604999. Assessment of the test-facility was enabled through financial supports of Agence Nationale de la Recherche (ANR, Project dEquipEx PHARE) and Conseil pour la Recherche Aeronautique Civile (CORAC - Programme CUMIN). Buildings and infrastructure were supported by Ecole Centrale de Lyon (ECL), instrumentations supported by Institut Carnot (INGENIERIE@LYON - Project MERIT). We are grateful for the continuous collaboration and financial support of SAFRAN AE since the beginning of this project and specifically for the present measurement campaign.

The authors are particularly grateful for the technical advice of the precious contributions of Benoit Paoletti, Gilbert Halter, Lionel Pierrard, Pierre Laucher and Sebastien Goguey.

References

1. M. Baumgartner, F. Kameier, and J. Hourmouziadis, *Non-Engine Order Blade Vibration in a High Pressure Compressor*, in Twelfth International Symposium on Airbreathing Engines, Melbourne, Australia, [Online]. Available: https://hal.archives-ouvertes.fr/hal-01353829 (Sep. 1995)
2. F. Kameier and W. Neise, *Rotating blade flow instability as a source of noise in axial turbomachines*, J. Sound Vibrat., **203**, no. 5, pp. 833–853, https://doi.org/10.1006/jsvi.1997.0902 (1997)
3. R. Mailach, I. Lehmann, and K. Vogeler, *Rotating Instabilities in an Axial Compressor Originating From the Fluctuating Blade Tip Vortex*, J. Turbomach. Trans. ASME, **123**, no. 3, pp. 453–460, doi: 10.1115/1.1370160 (2000)
4. J. März, C. Hah, and W. Neise, *An Experimental and Numerical Investigation into the Mechanisms of Rotating Instability*, J. Turbomach. Trans. ASME, **124**, no. 3, pp. 367–374, doi: 10.1115/1.1460915 (2002)
5. J. M. Tyler and T. G. Sofrin, *Axial Flow Compressor Noise Studies*, in SAE Technical Paper, doi: 10.4271/620532 (1962)
6. T. R. Camp, *A Study of Acoustic Resonance in a Low-Speed Multistage Compressor*, J. Turbomach. Trans. ASME, **121**, no. 1, pp. 36–43, doi: 10.1115/1.2841232 (Jan. 1999)
7. R. Parker and S. A. T. Stoneman, *The Excitation and Consequences of Acoustic Resonances in Enclosed Fluid Flow Around Solid Bodies*, Proceedings of the Institution of Mechanical Engineers, Part C: Mechanical Engineering Science, **203**, no. 1, pp. 9–19, doi: 10.1243/PIME_PROC_1989_203_081_02 (Jan. 1989)
8. A. J. Cooper and N. Peake, *Trapped acoustic modes in aeroengine intakes with swirling flow*, J. Fluid Mech., **419**, pp. 151–175, doi: 10.1017/S0022112000001245 (2000)
9. M. Vahdati and N. Cumpsty, *Aeroelastic Instability in Transonic Fans*, J. Eng. Gas Turbines Power – Trans. ASME, **138**, p. 022604 (2016)
10. S. T. Clark, *Design for coupled-mode flutter and non-synchronous vibration in turbomachinery*, Ph.D. Thesis, [Online]. Available: https://ui.adsabs.harvard.edu/abs/2013PhDT.....61C (Jan. 2013)
11. N. A. Cumpsty and D. S. Whitehead, *The excitation of acoustic resonances by vortex shedding*, J. Sound

Vibrat., **18**, no. 3, pp. 353–369, doi: 10.1016/0022-460X(71)90707-3 (Oct. 1971)
12. R. E. Kielb, J. W. Barter, J. P. Thomas, and K. C. Hall, *Blade Excitation by Aerodynamic Instabilities: A Compressor Blade Study*, in GT2003, **4**: Turbo Expo 2003, pp. 399–406, doi: 10.1115/GT2003-38634 (Jun. 2003)
13. C. Brandstetter, M. Jüngst, and H.-P. Schiffer, *Measurements of Radial Vortices, Spill Forward, and Vortex Breakdown in a Transonic Compressor*, J. Turbomach. Trans. ASME, **140**, no. 6, pp. 061004-061004–14, doi: 10.1115/1.4039053 (Apr. 2018)
14. S. Stapelfeldt and C. Brandstetter, *Non-synchronous vibration in axial compressors: Lock-in mechanism and semi-analytical model*, preprint, doi: 10.13140/RG.2.2.16519.75688
15. B. Hellmich and J. R. Seume, *Causes of Acoustic Resonance in a High-Speed Axial Compressor*, J. Turbomach. Trans. ASME, **130**, no. 031003, doi: 10.1115/1.2775487 (May 2008)
16. A.-L. Fiquet, C. Brandstetter, S. Aubert, and M. Philit, *Non-Synchronous Aeroacoustic Interaction in an Axial Multi-Stage Compressor*, J. Turbomach. Trans. ASME, **141**, no. 101013, doi: 10.1115/1.4044675 (Oct. 2019)
17. C. Brandstetter, B. Paoletti, and X. Ottavy, *Compressible Modal Instability Onset in an Aerodynamically Mistuned Transonic Fan*, J. Turbomach. Trans. ASME, **141**, no. 3, pp. 031004-031004–11, doi: 10.1115/1.4042310 (Jan. 2019)
18. M. Rodrigues, L. Soulat, B. Baoletti, X. Ottavy, and C. Brandstetter, *Aerodynamic investigation of a composite low-speed fan for UHBR application*, in ASME Turbo Expo 2020, doi: 10.1115/GT2020-14915 (2020)

Appendix

Based on the experimental observations, the signals corresponding to the convected phenomena result from random disturbances which appear at arbitrary times and decay as they travel around the circumference. The decay of these random disturbances must be limited. Otherwise multiples of the angular velocity Ω_a^S would not be visible in the pressure spectra.

Assuming, that a disturbance appears in the relative frame of reference at time t_d, for example due to boundary layer separation, travels around the circumference with Ω_a^S and decays over time with λ, its signature at one sensor position can be described as:

$$p^S(t > t_d) = \sum_{N_a=-\infty}^{\infty} A_{N_a}\, e^{-\lambda(t-t_d)} e^{i(-N_a \Omega_a^S t + \varphi_a)}$$

A measured signal can hence be interpreted as a sum of random disturbances appearing at random times, but with a specific decay rate depending on the underlying physical phenomenon.

Fig. 13 shows an artificial signal as a sum of random disturbances with constant initial amplitude of A=1, appearing with random phase and at random times at an average rate of 1 per revolution and a decay half-life of t_h=0.5 revolutions, hence: λ=log(2)/0.5.

Considering the Fourier transform of the auto-correlation function

$$r_{xx}(t) = \lim_{T\to\infty} \frac{1}{2T} \int_{-T}^{T} p\,(\tau)\overline{p(t+\tau)}\mathrm{d}\tau$$

the auto-spectral density is derived:

$$S_{XX}(\omega) = F(r_{xx})(\omega) = \frac{1}{2\pi}\int_{-\infty}^{\infty} r_{xx}\,(t) e^{-i\omega t}\mathrm{d}t$$

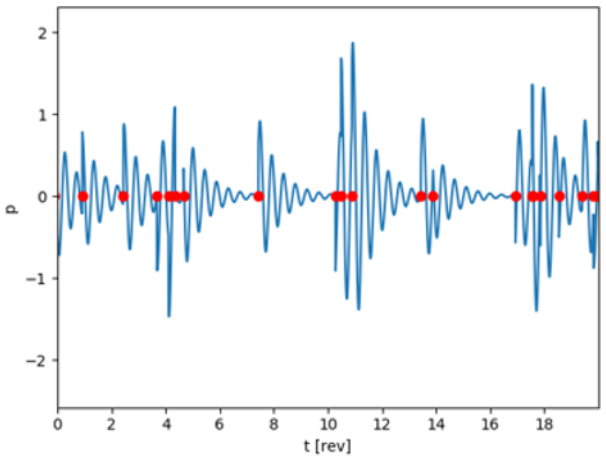

Fig. 13. Artificial signal consisting of decaying disturbances with constant initial amplitude occurring at random times (red dots)

With the right-handed side of this spectrum

$$G_{XX}(\omega) = 2S_{XX}(\omega)\ for\ \omega > 0$$

the coherence is calculated as :

$$C_{xy}(f) = \frac{|G_{xy}(f)|^2}{G_{xx}(f)G_{yy}(f)}$$

Calculating the coherence in sliding windows between the raw signal p_{raw}=p(t) and the time-shifted signal p_{shift}=p(t+Δt) the following dependency as a function of the decay half-life t_h is derived:

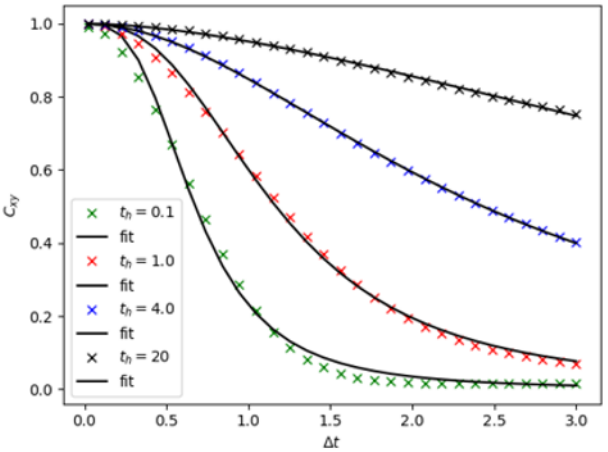

Fig. 14. Coherence of artificial signal for different time shifts in dependency of signal decay rate

The results have been fitted with a Hill-function in the form:

$$C_{fit}(\Delta t) = 1 - \frac{1}{1 + (\frac{a}{\Delta t})^b}$$

Coefficient a shows a monotonic rise with the half-life as depicted in Fig. 15, with a constant shift depending on the window size. It is found that this correlation is widely independent from the frequency of the disturbance and the average number of disturbances per revolution.
It can hence be used to determine the decay rate of a real signal spectrum, under the assumption that it is composed from a series of independent, random disturbances as described above.

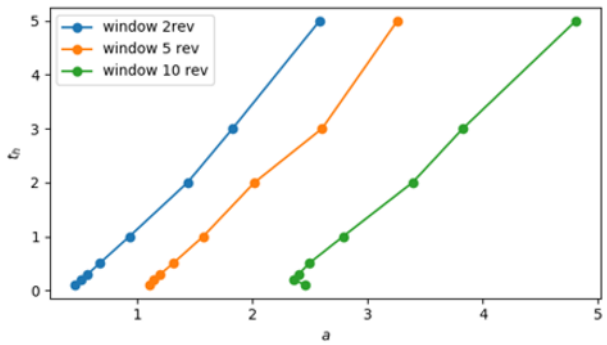

Fig. 15. Evolution of fit-parameter {a} for different window sizes and signal decay rates

If signals are correlated over time, for example due to interaction with periodic processes like blade vibrations, blade passing frequency, resonant acoustic modes, etc, the value for the half-life will increase.

Applied to the measurement discussed in this paper with the 16-bladed rotor, the spectrum shown in Fig. 16 is derived. Comparable results are derived if multiple sensors distributed around the circumference are considered by calculating the coherence based on cross-spectral-density.

As assumed from the dependency of the SWFT window size (Fig. 6), the most stable modes are those locked in to structural vibrations (7.54 and 8.46), their modulation with the *bpf*, the acoustic modes (11.79 and 12.76) and dominantly the blade passing frequency (16). For freely convected disturbances, a decay half-life of approximately 0.4 – 0.8 revolutions is determined.

Application of this method is based on many assumptions and must be validated in further studies. For the results of the semi-analytic model, the method derives accurate results. It has shown robust against parameters like the window size and operating point and derives coherent results that confirm the findings from this paper based on physical interpretations.

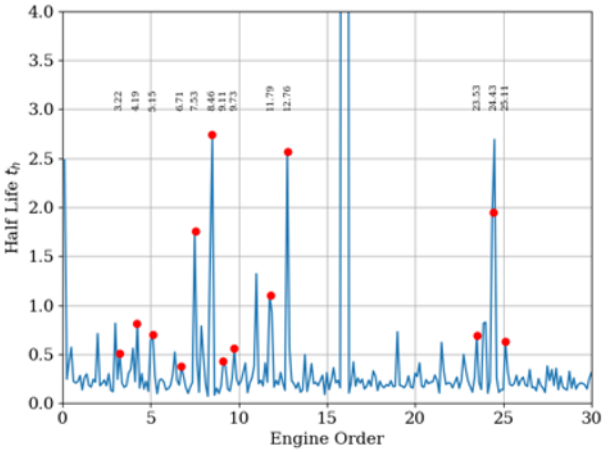

Fig. 16. Half-life spectrum for reference measurement of fan operating near-stall, calculated from sensor near leading edge